IAC-12-A3.5.1

THE MESSENGER MISSION CONTINUES: TRANSITION TO THE EXTENDED MISSION

Ralph L. McNutt, Jr.
The Johns Hopkins University Applied Physics Laboratory, U.S.A., ralph.mcnutt@jhuapl.edu

Sean C. Solomon
Department of Terrestrial Magnetism, Carnegie Institution of Washington, and
Lamont-Doherty Earth Observatory, Columbia University, U.S.A., scs@dtm.ciw.edu

Larry R. Nittler
Department of Terrestrial Magnetism, Carnegie Institution of Washington, U.S.A, nittler@dtm.ciw.edu

Peter D. Bedini
The Johns Hopkins University Applied Physics Laboratory, U.S.A., peter.bedini@jhuapl.edu

Eric J. Finnegan
The Johns Hopkins University Applied Physics Laboratory, U.S.A., eric.finnegan@jhuapl.edu

Helene L. Winters
The Johns Hopkins University Applied Physics Laboratory, U.S.A., helene.winters@jhuapl.edu

David G. Grant
The Johns Hopkins University Applied Physics Laboratory, U.S.A., david.grant@jhuapl.edu

and the MESSENGER Team
Various Institutions

The MErcury Surface, Space ENvironment, GEochemistry, and Ranging (MESSENGER) spacecraft, under NASA's Discovery Program, is the first probe to orbit the planet Mercury. Launched in August 2004, MESSENGER completed three flybys of Mercury that marked the first spacecraft visits to the innermost planet since those of Mariner 10 in 1974–1975. Following a successful orbit insertion on 18 March 2011, MESSENGER gathered data continually during its primary, yearlong mission. An extended mission, for an additional Earth year of operations from orbit, was approved by NASA and announced on 9 November 2011. Building on the scientific results to date from the primary mission, six new and more focused science questions were posed for the extended mission: (1) What are the sources of Mercury's surface volatiles? (2) How late into Mercury's history did volcanism persist? (3) How did Mercury's long-wavelength topography change with time? (4) What is the origin of localized regions of enhanced exospheric density on Mercury? (5) How does the solar cycle affect Mercury's exosphere and volatile transport? (6) What is the origin of Mercury's energetic electrons? As with the primary mission, each of these questions is linked to a specific set of measurement objectives designed to yield a corresponding answer. The six measurement objectives are, respectively: (1) determine the morphological and compositional context of "hollows" and their relationship to bright crater-floor deposits and pyroclastic vents; (2) acquire targeted, high-resolution observations of volcanic materials of low impact crater density identified during the primary mission; (3) document changes in long-wavelength topography through geological time on Mercury from altimetric and complementary imaging measurements; (4) characterize regions of enhanced exospheric density versus solar distance, proximity to specific geologic units, solar activity, and magnetospheric conditions; (5) measure changes in exospheric neutral species, plasma ions, and magnetospheric dynamics as solar activity increases; and (6) infer the sources and energization mechanism from the location, energy spectra, and temporal profiles of energetic electrons. Overarching themes as embodied in the science questions for the MESSENGER extended mission ensure that the second year of orbital operations is not simply a continuation of the primary mission. These themes include more comprehensive measurement of the magnetosphere and exosphere during a period of more active Sun, greater focus on observations at low spacecraft altitudes, and a greater variety of targeted observations. In particular, the extended mission is a critical epoch for the study of Mercury's magnetosphere and exosphere.

I. INTRODUCTION

On 18 March 2011, the MErcury Surface, Space ENvironment, GEochemistry, and Ranging (MESSENGER) spacecraft [1] became the first probe to orbit Mercury [2]. With this milestone MESSENGER commenced the year-long primary orbital phase of its mission, to have been followed by one year of data archiving and analysis, to 17 March 2013. After the

successful initiation of science operations, a MESSENGER extended mission (XM1) was proposed to take advantage of the presence of an operating spacecraft in orbit about the innermost planet to address scientific questions regarding Mercury, and Earth-like planets more generally, by making new measurements that extend and complement those taken during the primary mission. XM1, involving one additional Earth-year of orbital observations, was implemented by NASA following a Senior Review, and that new segment of operations is now underway.

Prior to MESSENGER's successful completion of its primary mission, it was expected on the basis of projections that sufficient propellant would remain to continue orbital operations for at least one additional Earth-year, and that proved to be the case [3]. For that reason, and because a second Earth-year of observations would permit a substantial advance in our understanding of Mercury beyond what will have been achieved at the end of the primary mission, the duration of XM1 was proposed to be one Earth-year. That the XM1 proposal could be assembled in advance of orbit insertion was because of the substantial return of information on the innermost planet achieved from the three Mercury flybys. Moreover, the development of the SciBox science-planning tool [4], already in extensive use for the primary mission, enabled effective planning of extended mission observations during the period of primary mission operations [5].

Several overarching themes for the MESSENGER extended mission ensured that the second year of orbital operations would not simply be a continuation of those of the primary mission. Those themes include operation during a more active Sun, greater focus on observations at low spacecraft attitudes, and a greater variety of targeted observations. The extended mission is permitting the only close-in observations of Mercury, to date or planned, near a maximum in the solar cycle. The lower average altitude has been accomplished by decreasing the nominal 12-hour orbital period of the primary mission to 8-hours by lowering the apoapsis of the orbit. The greater variety of instruments that will make targeted observations is enabled by the fact that the global mapping objectives of the primary mission have been accomplished.

I.I. Evolution of MESSENGER's Orbit

MESSENGER's primary mission of one year of orbital observations began from a nominal 12-h orbit, initially with a 200-km periapsis altitude, an 82.5° inclination, and 60°N periapsis latitude [3]. Since MESSENGER began orbital operations in March 2011, the gravitational pull of the Sun has worked to raise the spacecraft's periapsis altitude, requiring periodic orbit-correction maneuvers (OCMs) during the primary mission to reset that altitude to 200 km. The increase in periapsis altitude between successive orbits continued (but more slowly) after the orbit period was shortened from 12 h to 8 h early in XM1. Beginning in March 2013, the orbit plane will have progressed to a point that the effect of solar gravity will begin to lower periapsis altitude between successive orbits rather than raise it. Even without OCMs, the periapsis altitude will remain within the preferred range of 200–500 km until March 2014. After March 2014, small OCMs will be needed to maintain the altitude within an acceptable range. There is sufficient propellant remaining to continue orbital operations for approximately one additional year of operations thereafter, until March 2015 [3].

I.II. The Scientific Payload

The MESSENGER spacecraft accomplishes its scientific investigations with its payload of seven science instruments plus the telecommunications system for radio science (RS) [1]. The instruments include the Mercury Dual Imaging System (MDIS), which consists of an 11-color-filter wide-angle camera (WAC) and a panchromatic narrow-angle camera (NAC) mounted on a single-degree-of-freedom scan platform [6]; a Gamma-Ray and Neutron Spectrometer (GRNS), including Gamma-Ray Spectrometer (GRS) and Neutron Spectrometer (NS) sensors [7]; an X-Ray Spectrometer (XRS), including sensors that point at the planet and at the Sun [8]; a Magnetometer (MAG) [9]; the Mercury Laser Altimeter (MLA) [10]; the Mercury Atmospheric and Surface Composition Spectrometer (MASCS), which uses a common telescope for the Ultraviolet and Visible Spectrometer (UVVS) and the Visible and Infrared Spectrograph (VIRS) [11]; and an Energetic Particle and Plasma Spectrometer (EPPS), consisting of the Energetic Particle Spectrometer (EPS) and the Fast Imaging Plasma Spectrometer (FIPS) [12].

II. RESULTS FROM THE PRIMARY MISSION

Following publications of initial scientific results from the three flybys of Mercury (e.g., [13-15]), the primary MESSENGER mission results continue to be documented in the scientific literature following initial presentation at scientific conferences and meetings and initial reports [16-22].

Following the preliminary design review for the mission in 2001, a set of success criteria was instituted and approved by the NASA Associate Administrator for Space Science on 20 June 2001. These "full mission success criteria," listed in Table I, were included as the Program Level Requirements (PLR) for the MESSENGER Discovery Project in Appendix 7 to the Discovery Program Plan. By the conclusion of MESSENGER's primary mission, all of these criteria had been successfully accomplished and documented via these publications and data deliveries to NASA's Planetary Data System (PDS) [23].

Criterion	Task
1	Provide major-element maps of Mercury to 10% relative uncertainty on the 1000-km scale and determine local composition and mineralogy at the ~20-km scale.
2a	Provide a global map with >90% coverage (monochrome) at 250-m average resolution and >80% of the planet imaged stereoscopically.
2b	Provide a global multispectral map at 2 km/pixel average resolution.
2c	Sample half of the northern hemisphere for topography at 1.5-m average height resolution.
3	Provide a multipole magnetic-field model resolved through quadrupole terms with an uncertainty of less than ~20% in the dipole magnitude and direction.
4	Provide a global gravity field to spherical harmonic degree and order 16 and determine the ratio of the solid-planet moment of inertia to the total moment of inertia to ~20% or better.
5	Identify the principal component of the radar-reflective material at Mercury's north pole.
6	Provide altitude profiles at 25-km resolution of the major neutral exospheric species and characterize the major ion-species energy distributions as functions of local time, Mercury heliocentric distance, and solar activity.

Table I: MESSENGER Primary Mission Full Mission Success Criteria

With respect to criterion 1, gamma-ray spectroscopy has provided 38,479 individual gamma-ray spectra, including 15,397 spectra acquired at low altitude (<2,000 km), which are the "prime" GRS science data (equivalent to 263 hours of low-altitude data). From these data the following major-element maps have been derived: silicon, <10% error poleward of 35°N, resolution <1000 km; oxygen, 10% to 15% error poleward of 34°N, resolution <1000 km; and potassium, <10% error poleward of 35°N, resolution <1000 km (Fig. I) [17].

Infrared spectroscopy has provided insights into local composition with 83.2 % coverage (as of 15 April 2012) at 20 km / pixel average (1,956,964 base map footprints). However, there is no clear evidence of the 1 μm band associated with ferrous iron in silicates. Lack of this absorption and evidence of ultraviolet (UV) absorption shortward of 300 nm is consistent with very low ferrous iron content (2–4 wt% FeO) [24].

Coverage of regions by planet-pointing X-ray spectrometers during times of solar X-ray activity has shown iron and titanium to be lower than expected, whereas sulfur is higher than expected [16].

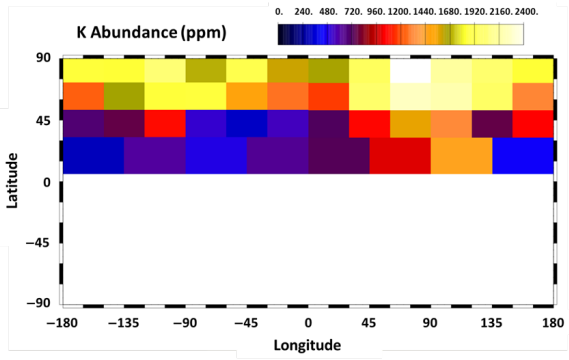

Fig. I: Potassium abundance in parts per million (ppm) poleward of 20°N latitude.

With respect to criterion 2, the primary mission has yielded a global monochrome map with 99.9 % coverage at 163 m / pixel average for the base map (34,834 images) and stereoscopic imaging with 92.5 % coverage (both as of 28 March 2012) at 168 m/pixel average (18,925 images). A global multispectral map has been produced with 99.8 % coverage (as of 28 April 2012) at 883 m/pixel average with 8 filters (5,146 color cubes) (Fig. II).

By 24 April 2012, 11,738,459 laser shots from the laser altimeter had been downlinked from orbit. At a spacing of 0.5° × 0.5°, 70 % of the northern hemisphere has been ranged at least once, and at a spacing of 0.25° × 0.25°, 51.4 % of the northern

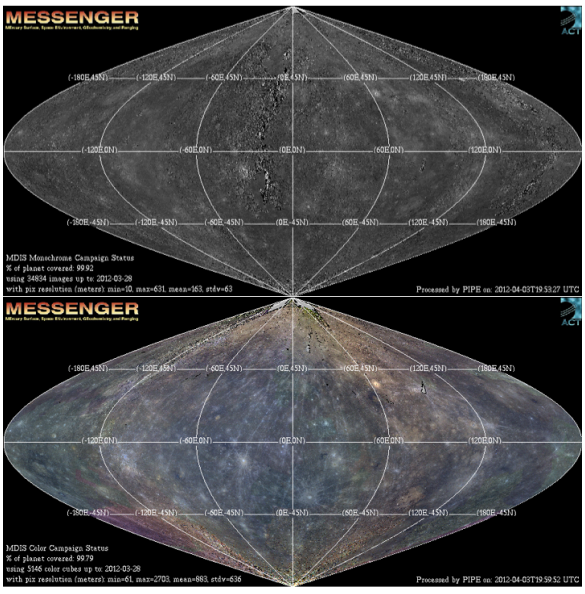

Fig. II: Global monochrome map (top) and global multispectral map (bottom).

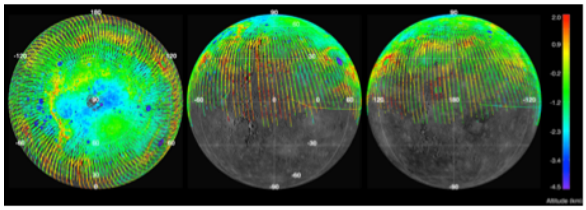

Fig. III: Topographic coverage maps by the MLA at the end of the primary mission. The northern hemisphere is to the left and the east-west hemispheres centered on 0° and 180° E longitude are in the center and to the right, respectively.

hemisphere has been ranged at least once, providing a topographic model of the northern hemisphere of the planet (Fig. III) [25]. The demonstrated precision in flight, neglecting ground response, slope, and other effects not present in the two-way (cruise) experiment, is 0.44 m root mean squared (RMS), from the root-summed-square of transmit and receive timing uncertainties of 2.93 ns [26]. Imaging and altimetry have together shown that widespread volcanism has been important in Mercury's geologic history [18] and have revealed "hollows," fresh-appearing, rimless depressions, commonly with high surface reflectance and often with bright halos. The host rocks are interpreted to have been excavated from depth by impact, and likely formation mechanisms involve recent loss of volatiles through pyroclastic volcanism, outgassing, sublimation, or space weathering [19].

With respect to criterion 3, the internal magnetic field of Mercury has been demonstrated to exhibit the form of a magnetic dipole, anti-parallel to the planet's spin axis but offset northward of the center of Mercury by 484 ± 11 km, on the basis of crossings of the magnetic equator. The dipole moment is 195 ± 10 nT-R_M^3, where R_M is Mercury's radius, and the tilt of the dipole from the spin axis is less than 2.5° [20].

With respect to criterion 4, an initial gravity model to degree and order 20 (designated HgM002, Table II) has been completed [27] and continues to be refined with the ongoing tracking data from the extended mission. From these data in conjunction with recent measurements of Mercury's obliquity and libration [28] and ancillary data [29], the ratio of the moment of inertia of Mercury's solid outer shell to that of the planet has been determined [30] to be $C_m/C = 0.452 \pm 0.035$ (15% at 2 standard deviations). Ongoing modeling and refinement of parameters suggest that a dense layer (possibly solid FeS) may overlie a liquid iron-rich outer core, a structure consistent with strongly reducing conditions. The core–mantle boundary may therefore be shallower than the ~410 km depth to the top of the fluid outer core.

Parameter	Value	Uncertainty
GM (km^3 s^{-2})	22,031.780	±0.02
C_{20}	-2.25×10^{-5}	$\pm 1 \times 10^{-7}$
C_{21}	-4.64×10^{-8}	$\pm 5 \times 10^{-8}$
S_{21}	1.35×10^{-8}	$\pm 5 \times 10^{-8}$
C_{22}	1.253×10^{-5}	$\pm 1 \times 10^{-7}$
S_{22}	5×10^{-8}	$\pm 1 \times 10^{-7}$
C_{30}	-4.49×10^{-6}	$\pm 3 \times 10^{-6}$
C_{40}	-6.5×10^{-6}	$\pm 8 \times 10^{-7}$

Table II: Selected (normalized) low-degree gravity coefficients in the HgM002 gravity model [27].

With respect to criterion 5, the combination of permanent shadows [31, 32], near-infrared reflectance [33], and inferred temperature distributions [34] are all consistent with long-term storage of water ice and other frozen volatiles in radar-bright regions.

With respect to criterion 6, the major neutral exospheric species have been identified as sodium, calcium, and magnesium, and 14 profiles of Na, Ca, and Mg have been acquired over the poles with ≤ 25-km altitude resolution. There have also been controlled-pointing dayside limb scans with coarser altitude resolution, including 1206 altitude profiles of Na, 1185 altitude profiles of Ca, and 1187 altitude profiles of Mg. The statistics for the three major species are similar. Five ion species have been characterized for three Mercury years, including H^+, He^{2+}, He^+, the O-group (O^+, water group), and the Na-group (Na^+, Mg^+, Si^+); and the spatial and temporal behavior of the ionized exosphere–magnetosphere system has been documented [21].

III. PLANNING THE EXTENDED MISSION

The MESSENGER extended mission has afforded an opportunity to observe the Mercury system under higher rates of imposed solar activity than during either the flybys or the primary mission (Fig. IV).

By spanning a portion of the solar cycle not heretofore viewed at close range at Mercury, observations from the extended mission are markedly improving our ability to distinguish among proposed exospheric source processes, and the range in behavior of Mercury's extraordinarily dynamic magnetosphere can be much more fully characterized. Increased solar activity corresponds to orders of magnitude greater variability in solar extreme ultraviolet (EUV) and X-ray emissions and solar energetic particle fluences, as well as a factor of 100 greater variation in solar wind forcing. XM1 occurs during a critical epoch for the study of Mercury's magnetosphere and exosphere, one that was not sampled by Mariner 10 and was not observed by MESSENGER through the primary mission.

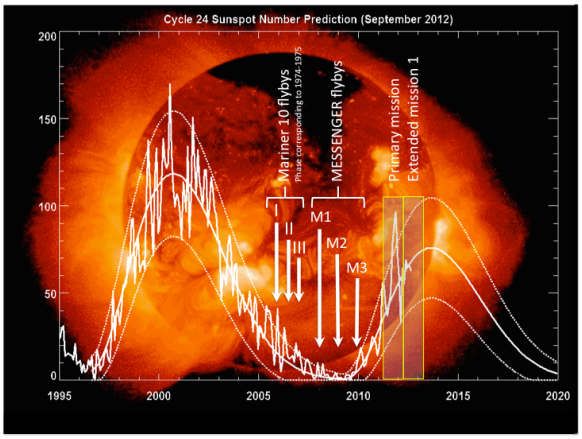

Fig. IV: Sunspot number for solar cycle 23 and the beginning of cycle 24. The three MESSENGER flybys occurred during a historically deep solar minimum and the three Mariner 10 flybys occurred during the declining phase of cycle 20.

Moreover, because Mercury is the only solar system analog of rocky extrasolar planets orbiting near their host stars, it is of great interest to understand the broadest possible range of behavior at Mercury so that we can better interpret signatures of analogous extrasolar planets. A campaign of targeted observations during which EPPS or UVVS controls spacecraft pointing is permitting MESSENGER to address source, loss, and transport processes for plasma and energetic particles within Mercury's magnetosphere and for neutral species in the exosphere with measurements not possible during the primary mission.

Improved spatial resolution of compositional measurements of Mercury's surface materials has been made possible during XM1 by means of changes in both mission design and observing strategies. At the beginning of XM1, two orbit-correction maneuvers (OCMs) were employed to reduce the orbital period to 8 h at a time when periapsis altitude was 278 km [3]. The lower average periapsis altitude that resulted has yielded an increase in measurement time below 300 km, for instance, increasing the sensitivity and resolution of elemental abundance measurements for spectral and morphological units on regional scales. The expansion in measurements of shorter-wavelength components of Mercury's gravity field is providing improved insight into the nature of isostatic support of topography on Mercury. Extended mission measurements are also resulting in an improved accuracy in the higher-order structure of Mercury's internal magnetic field, diagnostic of competing models for internal field generation. An improved context for these measurements is being provided by color imaging of the northern hemisphere using fewer filters but the full spatial resolution of the MDIS instrument.

Targeted observations during the extended mission are more frequent than during the primary mission, and those targeted observations are being made with more of MESSENGER's instruments to address a greater variety of planetary processes. An emphasis during the primary mission on the production of global maps limited opportunities for targeted observations for instruments other than MDIS that required changes in spacecraft pointing. During XM1, MLA has been making off-nadir observations of targets of high geological interest, such as candidate volcanic centers, fault structures, and impact craters. A greater range of extended-duration and directed observations by the MASCS instrument is addressing questions of surface mineralogical variations and exospheric dynamics beyond those that could be addressed during the primary mission.

III.I. Geology Objectives

The MESSENGER extended mission is allowing science questions posed for the primary mission to be addressed in substantially greater depth with new and complementary measurements. Measurements acquired during XM1 are also improving the resolution of MDIS global mapping; filling gaps in MDIS global coverage; improving the accuracy and coverage of MLA and MDIS terrain models; improving the resolution, coverage, and quality of MASCS and XRS spectral mapping; and expanding the number of targeted observations. Discoveries during the primary mission are providing new targets for more focused study during the extended mission.

New measurement campaigns complementary to those of the primary mission include four new MDIS data sets and one new UVVS data set. Continuation of MLA and VIRS global mapping is increasing coverage density of spectral and topographic measurements, and continuation of XRS and NS measurements is increasing the spatial and spectral resolution of elemental abundance measurements. Many of these measurements were not possible during the primary mission because of limitations in the observing schedule and spacecraft and downlink resources.

III.I.I. New MDIS Measurement Campaigns

Terrain modeling is being improved by collecting two new MDIS global maps at resolutions comparable to those of the primary mission's panchromatic mosaic (the "base map") and its stereo complement, but at different geometries: a global WAC/NAC map at <250 m/pixel spatial resolution, for which solar incidence angle is minimized by using

higher-Sun opportunities similar to those used for color mapping; and a second off-nadir geometry, taken at the same local solar time as the base map and its primary mission stereo complement, except with the viewing geometry "flipped" from the primary mission's stereo complement (e.g., areas observed off-nadir during the primary mission looking "up" the ground track will be observed during the extended mission looking "down" the ground track). Together, the four geometries enhance stereo-derived terrain models.

MDIS is also completing two regional campaigns. North polar mapping analogous to the south polar mapping conducted during the primary mission covers latitudes poleward of 70°N at a variety of solar azimuths, to better constrain locations of permanently shadowed regions within which enhanced hydrogen concentration may be detected by NS. MDIS is obtaining a three-color map of the northern hemisphere at low solar incidence angle and at the full ~150 m/pixel native resolution of the WAC, increasing the ability to resolve compositional variations by a factor of ~6.

III.I.II. UVVS Southern Hemisphere "Map"

UVVS is carrying out sustained observations of several thousand southern hemisphere locations laid out in a regular pattern, to compile a UV "sampling grid" of the major units. UVVS spectra covering the wavelength range 220–320 nm are being taken in coordination with VIRS spectra at 300–1440 nm to provide a rich set of mineralogical measurements. Full MASCS spectra require 35–40 s of dwell time on a fixed spot to obtain both VIRS and UVVS spectra; limitations in the spacecraft slew rate to track these spots restrict this measurement type to higher altitudes over equatorial and southern regions.

III.I.III. Targeted MDIS, MLA, and VIRS Observations

New targeted observations cover key volcanic and tectonic features and craters, particularly with northern hemisphere NAC high-resolution strips and VIRS profiles. The extended mission will double the density of coverage by VIRS and MLA, supporting higher spatial-resolution determinations of visible and near-infrared spectral variations and high-accuracy elevations.

III.I.IV. Vulcanoid and Satellite Search

At high altitudes over the southern hemisphere, MDIS has substantial unused observing time. This time is being used to enhance the four cruise imaging campaigns to search for asteroids orbiting the Sun within the orbit of Mercury ("vulcanoids") [35] as well as possible satellites of Mercury. This search is being conducted on a non-interference basis with other observations.

III.II. Geochemistry Objectives

In the MESSENGER extended mission, the geochemical instruments focus on resolving low-abundance species and improving the spatial resolution for more abundant species. Elemental abundance identifications depend critically on counting statistics. The counting statistics and spatial resolution both depend on the detection efficiency for a given element, the distance to the planet, counting times, and, in the case of XRS, the time-variable solar X-ray flux. For these instruments, key advantages of the extended mission are the use of an 8-h orbit and the second year of counting time (which improves counting statistics), both of which allow substantially better spatial resolution for maps of elemental composition.

For the extended mission, NS measurements are enhanced through an increased counting time and lower average altitude (due to the 8-hour orbit). The NS data therefore have improved statistical accuracy, increased signal-to-background due to the lower average altitude, and improved spatial resolution, also from the lower average altitude. These measurement improvements result in reduced uncertainties both in the delineation of compositional provinces and in quantitative abundance estimates. Specific areas of improvement include the following: (1) The increased time and improved spatial resolution give an improvement in non-polar mapping. (2) The improved statistical precision enhances algorithms used for increasing the NS spatial resolution. (3) Substantially better characterization of the radar-reflective materials in polar regions and the distribution of H at high northern latitudes are also following from the additional time, lower averaged altitudes, and high-inclination orbit.

The XRS measures fluorescent emissions from the planet's surface due to excitation by X-rays emitted from the Sun's corona. Thus, the detected signal depends critically on the solar X-ray flux, which varies markedly in time in both flux and spectral shape. Under "quiet-Sun" conditions, the solar X-ray flux allows measurement of Mg, Al, and Si. Low count rates under such conditions require summing large numbers of spectra to obtain statistically significant results (work that is ongoing), thereby decreasing spatial resolution. The extended mission has allowed for increased integration times at low altitudes, providing for smaller statistical uncertainties and better resolution of these elements on regional scales.

During solar flares, the solar flux greatly increases and its spectrum hardens, allowing detection of

elements of higher atomic number such as S, Ca, Ti, and Fe within relatively short periods of time (hence enhancing spatial resolution, e.g., <100 km at low spacecraft altitude). The occurrence of solar flares correlates with the solar cycle; as the activity level of the Sun increases, so do the frequency and intensity of flares. The current solar cycle has started later than anticipated, following a period of unusually low solar activity in 2008–2009 (Fig. IV). The primary orbital mission ended prior to the next solar maximum, now predicted to occur near the end of 2013. On the basis of statistics from the previous solar cycle, we can expect approximately twice the number of solar flares during the extended mission as during the primary mission. Therefore, the extended mission is expected to more than double the XRS data set for S, Ca, Ti, and Fe, greatly increasing the chances of obtaining good elemental data for these elements for a broad range of geologically interesting targets. Moreover, the quiet-Sun X-ray flux also increases with the solar cycle, and the extended mission is improving the Mg, Al, and Si data as well.

III.III. Geophysics Objectives

Extended mission goals for geophysics include improving knowledge of the structure, dynamics, and evolution of Mercury by increasing the coverage, spatial resolution, and signal-to-noise ratio (SNR) of observations obtained in the primary mission. The most important factor for the geophysics investigation is the frequency of periapsis-lowering OCMs. To preserve the objective of global imaging and to permit greater flexibility in off-nadir pointing and ranging to the north polar region, periapsis altitude during the primary mission was allowed to drift higher than ideal for gravity observations. The baseline trajectory for the extended mission is maintaining a lower average periapsis that optimizes the gravity observations and also has greater flexibility to orient the spacecraft to maximize Doppler tracking observations.

III.III.I. Fine Structure in the Gravity Field

The extended mission provides an ideal opportunity to focus on higher-precision and shorter-wavelength observations of the gravity field. Increased precision greatly improves knowledge of planetary structure. Fine-scale structure in the gravity field allows clear identification of mass anomalies associated with impact basins (e.g., Caloris) and other large-scale features and improves estimates of variations in crustal thickness [25, 27]. An additional year of range-rate data should improve the signal quality in the gravity field model by ~40%, revealing new details of the relationship between subsurface density and topography. There is potential for a marked improvement in the quality of range-rate data. The near 4:1 ratio between the orbit periods of Earth and Mercury prevents regions at longitudes 180–300°E, for which the Mercury-Sun-Earth (MSE) angle exceeds 120°, from being viewed at an ideal geometry during the primary mission. This problem can be mitigated during the extended mission by turning the spacecraft to optimize SNR for MSE angles between 60° and 120°.

III.III.II. Topography of High-interest Geological Features

During the primary mission, the top priority for MLA observations was to construct a topographic grid of the northern hemisphere of Mercury [25]. Excursions to profile areas of polar deposits near the north pole represented the only targeting for MLA observations during the primary mission. During the extended mission, MLA is using off-nadir profiles to investigate geological features of high interest, including volcanic vents, major tectonic features, and areas of any crustal magnetic anomalies. Because topographic data retain signatures of formative geophysical processes, these observations are crucial to establish the underlying structures and origin of key geological features.

III.III.III. Higher-order Structure in the Magnetic Field

The extended mission is being used to improve greatly the accuracy of the higher-order structure of the planetary magnetic field. The longer time series improves the statistics and reduces the detection limits on possible secular variation by at least half.

III.IV. Magnetosphere Objectives

The overarching magnetospheric science objective for the extended mission is to address the question: What are the dynamics exhibited by Mercury's magnetosphere? The key observational objective has been to customize spacecraft pointing to maximize EPPS pitch angle coverage. For FIPS, this flexibility allows assessment of distribution functions to identify source and loss processes and to measure plasma flows. Flows are essential to quantify energetics, because, together with the magnetic field, flows determine the electric field and hence electric potentials. For EPS, this pointing control enables assessment of the entry and loss mechanisms for solar energetic particles and ensures coverage of acceleration processes within Mercury's magnetosphere. The magnetospheric observations are addressing the following corollary topics:

III.IV.I. Plasma and Magnetic Flux Transportation under Extreme Forcing

Plasma transport reflects the intense dynamics driven by the solar wind–planetary magnetic field interaction. Combining magnetic field and plasma measurements in dayside reconnection flows, on the nightside, and during episodic reconnection and plasmoid formation allows determination of the concomitant flux transport of each process and the measurement of the electric fields and energetics of each.

(1) How much energy does solar wind plasma acquire in dayside reconnection flows? This quantity is measured by turning the spacecraft so that the FIPS field of view (FOV) is directed toward the subsolar point to observe flows tangent to the magnetopause associated with magnetic reconnection.

(2) Are impulsive reconnection events Earth-like substorms? Intense reconnection events occur episodically in the tail, and if they are associated with particle precipitation there should be UV or visible emissions from near the surface. We are searching for "auroral" emissions using long-eclipse orbits to point MASCS and MDIS toward the surface.

(3) Does magnetic flux return to the dayside around the planet, or is flux transported through the non-conducting outer layers of the planet? Magnetospheric convection implies flows that return magnetic flux from the tail to the dayside. If flux is transported through the outer layers of the planet, there would be persistent and intense deposition of plasma to the surface at all latitudes. To distinguish among possibilities, we place a portion of the FIPS FOV as close to anti-sunward as possible within Sun keep-in constraints; these observations are ongoing.

III.IV.II. Source, Loss, and Precipitation Processes

Determining entry mechanisms, the evolution of plasmas during wave–particle interactions, and precipitation losses requires pointing FIPS to observe distribution functions. The best distributions are now being obtained by rolling the spacecraft about the spacecraft–Sun line to sweep out the maximum possible solid angle.

III.IV.III. Solar Energetic Particles Transport and Internal Particle Acceleration Processes

Solar energetic protons gain ready access to the surface, but energetic electrons are affected by the magnetic field and its linkage with the solar wind. By optimizing EPS pitch angle coverage, we identify the access mechanisms for energetic electrons. Extreme solar wind conditions also allow us to monitor all dynamical states of the system for internal acceleration processes.

III.IV.IV. Source Regions of Heavy Ions and Their Drivers

Source regions of heavy ions are clearly indicated by their distribution functions. To establish the origins of heavy ions, we measure the heavy ion distribution functions by the systematic pointing of FIPS; these observations are also ongoing.

III.V. Exosphere Objectives

To characterize exospheric dynamics, we are now devoting substantial spacecraft pointing time to UVVS observations in several campaigns so that variations in emissions can be unambiguously related to solar EUV and X-ray fluence, magnetospheric dynamics, or solar energetic particles. There are six pointing scenarios: (a) Regular limb scans close to the planet (spacecraft altitudes <2000 km); (b) directed limb scans over surface areas of geological interest; (c) observations directed at regions of enhanced exospheric density; (d) full 360° spacecraft rolls about the Sun–Mercury line, particularly while in shadow; (e) campaign-style observations in which MASCS controls pointing over periods of time; and (f) observations during which the MASCS FOV is continuously circled around the planet to sample a full 360° around the limb during dawn–dusk and noon–midnight orbits.

These observations provide the data to address the following topics:

III.V.I. Localized Structures

(1) What leads to the equatorial-dawn enhancement of Ca? (2) Is this unique to Ca? (3) Are exospheric sources tied to geological features? (4) What is the distribution of low-energy species near the surface? Observations that probe all directions over a short time span (scenario f) address questions 1 and 2. Low-altitude dayside limb scans (scenario a) and directed observations (scenario b) are needed to reveal exospheric source connections to surface features. Viewing the terminator from the anti-Sun direction (scenario d) is the only definitive way to resolve question 4.

III.V.II. Polar Regions

(1) What are the controlling source mechanisms over the polar regions? (2) What species are adsorbed at high latitudes? (3) Why are the polar-region altitude distributions of Na, Ca, and Mg different from one another? Polar observations of the exosphere were limited to only eight orbits in the nominal mission, corresponding to a total observation time of only a few hours. To resolve these questions, these polar-region scan campaigns have been extended over many sequential orbits (scenarios b and e) during XM1.

III.V.III. Exosphere-magnetosphere Connections

(1) How is material transported to the tail? (2) What are the relationships between neutrals and their ions? (3) What is the exosphere's response to changes in the IMF? Studying transport processes, tracking the development of ions from neutral antecedents, and capturing variations in the exosphere with changes in the IMF, EUV and X-ray fluence, and solar energetic particle flux all require observations continuously repeated around the planet (scenarios e and f).

III.V.IV. Source Processes

(1) To what degree does meteoroid impact vaporization contribute to the exosphere? (2) Are two-stage release processes important? (3) Are exospheric species ejected in excited states? A campaign (scenario e) of leading- and trailing-hemisphere exosphere observations before, during, and after known meteor streams is needed to resolve question 1. Searches for the signatures of two-stage source processes and excited atomic species require campaigns with continuous viewing (scenarios c and e).

III.V.V. Weak Emission Signatures

(1) What are the distributions of weakly emitting species? (2) What are the distributions of less-dense species? Quantification of such species (O, OH, S, Al, Fe, Ti, Ni, Cl, and Mn) is critical to distinguish among different surface mineral assemblages consistent with other observations and requires extended-duration observations focused near the surface (scenario a) and on regions of the highest densities (scenarios c and e).

IV. XM1 SCIENCE QUESTIONS

As with the primary mission, the plans for the extended mission can be stated succinctly in terms of six science questions, each of which has a corresponding measurement objective and implementation strategy.

IV.I. What are the sources of surface volatiles?

The discovery of the "hollows" in the primary mission has raised the question of their potential relationship to the volatile materials that supply both the exosphere and magnetosphere with material on a continuing basis. The corresponding measurement objective is to *determine the morphological and compositional context of "hollows" and their relationship to bright crater-floor deposits and pyroclastic vents* (Fig. V). The required measurements include: (1) repeated coverage of given targets for change detection, (2) characterization of hollows through high-resolution targeted

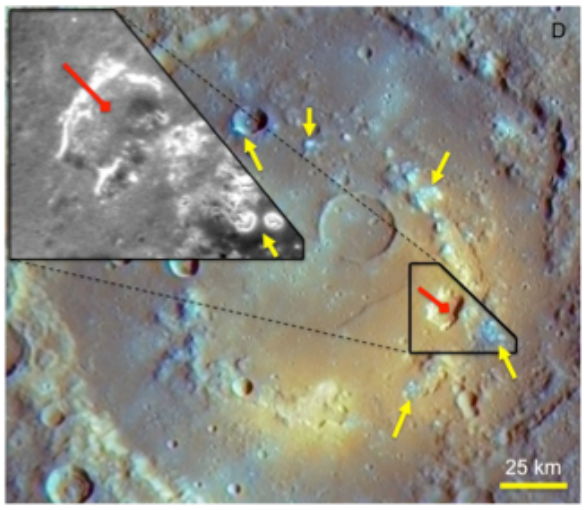

Fig. V. Praxiteles crater in exaggerated color; yellow arrows denote hollows, which appear blue in the image. The red arrow indicates a likely volcanic vent. The inset shows details of the depressions [19].

monochrome imaging, (3) increased spectral resolution for global compositional mapping, (4) mineralogical and compositional measurements by VIRS, XRS, and GRNS at an increased signal/noise ratio, and (5) targeted topography measurements.

IV.II. How late into Mercury's history did volcanism persist?

Extensive volcanism on Mercury, hinted at by Mariner 10 observations [37] but confirmed by MESSENGER on its first flyby of the planet [38, 39], is now understood to have been a major influence of the early geological history of Mercury [18]. Observations from the primary mission reveal variations in the size–frequency distributions of impact craters on volcanic deposits, information that provides insight into how late volcanic activity persisted. To address this question, the corresponding measurement objective is to *acquire targeted, high-resolution observations of volcanic materials of low impact crater density identified in the primary mission* (Fig. VI). Measurements include: (1) increased spectral and spatial resolution for compositional mapping, (2) targeted high-resolution color and monochrome imaging for crater density measurements, and (3) targeted topography measurements.

IV.III. How did Mercury's long-wavelength topography change with time?

The combination of high-resolution imaging and topographic mapping of the northern, smooth plains [18] and surrounding areas show extensive variations in long-wavelength topography subsequent to plains

emplacement and channel formation [25]. Such variations were not known prior to the MESSENGER primary mission. This question, raised by the primary mission, provides an opportunity to reveal new aspects of mantle dynamics and the global response to interior cooling and contraction. The corresponding measurement objective in this case is to *document changes in long-wavelength topography versus geological time on Mercury from altimetric and complementary imaging measurements* (Fig. VII). Enabling measurements include: (1) targeted altimetry of volcanic flow features to seek changes in "downhill" directions, (2) higher-resolution determination of the northern hemisphere gravity field from the lower average spacecraft elevation near periapsis, and (3) targeted imaging to document the deformational history of long-wavelength topographic variations to compare with predictions from mantle convection and global contraction models.

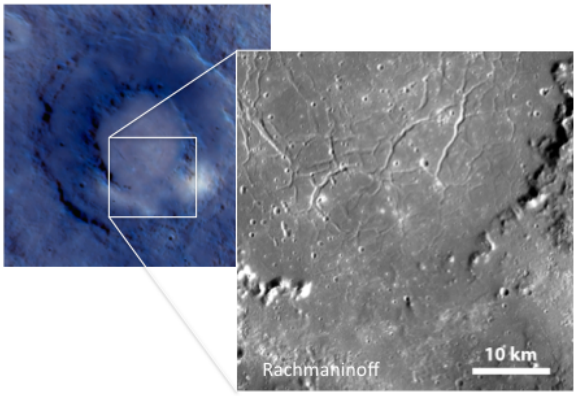

Fig. VI: The lightly cratered floor of the Rachmaninoff basin was discovered from images taken on MESSENGER's third flyby of the planet prior to orbit insertion [40]. The exaggerated-color image from the flyby shows relatively uniform spectral properties. The inset from the orbital mission reveals details of the basin floor, including the low density of craters emplaced subsequent to basin formation.

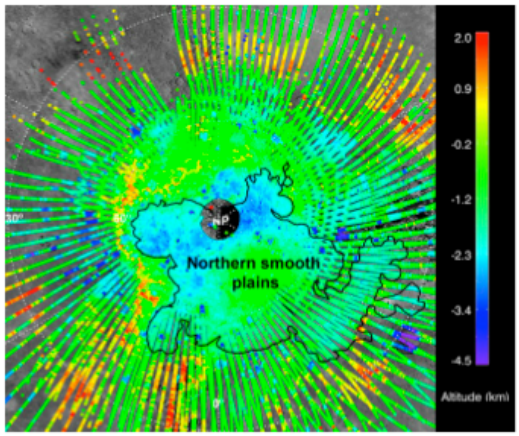

Fig. VII: Topographic map of Mercury's northern smooth plains from MLA. Relative altitude is shown in the scale to the right.

IV.IV. What is the origin of localized regions of enhanced exospheric density?

The major constituents of the exosphere of Mercury have been well characterized, beginning with the three flybys [41-43] and continuing with the primary mission for which viewing geometries have different constraints. Nonetheless, these observations have brought to light new scientific puzzles in the distribution of exospheric material that can be addressed only with the more varied observation geometries allowed by XM1. The most pressing feature is characterized by unanticipated density enhancements, which may be related to solar activity, geologic formations (e.g., hollows), or both, and so the measurement objective is to *characterize regions of enhanced density versus solar distance, proximity to geologic units, solar activity, and magnetospheric conditions* (Fig. VIII). Enabling operations include (1) campaigns to probe enhanced-density regions from diverse viewpoints over multiple orbits and to conduct synoptic observations throughout the Mercury year, and (2) increased observation time at low altitudes to explore connections between surface source regions and regions of enhanced density.

IV.V. How does the solar cycle affect Mercury's exosphere and volatile transport?

The two evolving variables upon which there is no control are the drifts in orbital parameters of MESSENGER, especially the latitude of periapsis and orbital inclination, and the phase of the solar cycle. The former is a function of available propulsive capability, but the inclination and periapsis latitude have not been and will not be changed by propulsion on board [3], as such changes are prohibitively expensive in propellant. The evolving

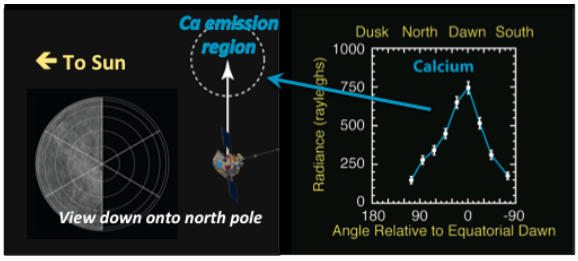

Fig. VIII: Schematic showing the region of enhanced emission from neutral calcium (left) and the associated intensity as a function of scan angle (right).

phase of the solar cycle has already revealed different phases of Mercury's magnetosphere from the flybys through the primary mission [44-47]. Such extreme variations suggest that correspondingly substantial variations could occur over the solar cycle with respect to transport of volatiles and the evolution of the exosphere. Hence, the fifth measurement objective for XM1 is to *measure changes in exospheric neutrals, plasma ions, and magnetospheric dynamics as solar activity increases* (Fig. IV). This objective is enabled by (1) higher solar activity yielding more than a factor of 10 greater variability in solar forcing, (2) dedicated spacecraft pointing to measure exospheric distributions at all local times on individual orbits, and (3) dedicated spacecraft pointing to optimize plasma flow (electric field) observations.

IV.VI. What is the origin of Mercury's energetic electrons?

From the first reported observations of energetic particles at Mercury during the first flyby of that planet by Mariner 10 [48], the interpretation of those observations was controversial [49]. The situation remained controversial throughout the MESSENGER flybys, although XRS observations suggested the presence of energetic electrons [50]. Only with the commencement of the primary mission were energetic electrons observed with regularity as a permanent feature of Mercury's magnetosphere [22, 51]. Although the MESSENGER observations of the primary mission have identified definitively the energetic particles observed by Mariner 10 as solely electrons and answered the question of the lack of observations during the MESSENGER flybys as the consequence of the near-equatorial flyby trajectories versus the organization of the electrons by the northwardly offset magnetic field of the planet. However, the observations of the primary mission have not resulted in the elucidation of the origin of this population. Hence, the final measurement objective for XM1 is to *infer the sources and energization mechanism from the location, energy spectra, and temporal profiles of energetic electrons* (Fig. IX). Observations made during the primary mission have shown the synergy of energetic electron signatures in multiple instruments on the payload, and so the enabling observations are (1) observations at all local times during changing solar activity, (2) coordinated measurements with low-energy data in XRS and GRNS sensors, and (3) tracking context with varying magnetospheric activity as revealed by magnetic field and plasma measurements (MAG and FIPS).

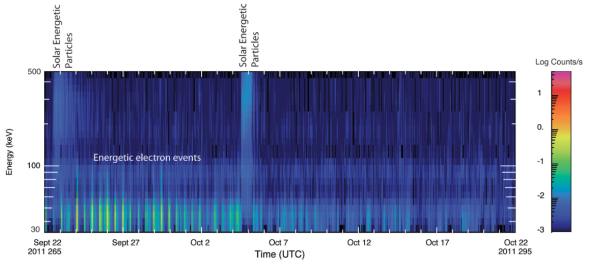

Fig. IX. Energy-time spectrogram showing 30 days of coverage (22 September – 22 October 2011) of energetic electron spectra. The electron signatures are quasi-periodic and more intense during the first half of this period between two sets of solar particle events.

V. EXTENDED MISSION ACCOMPLISHMENTS TO DATE

Following approval of the MESSENGER extended mission, success criteria were documented in "Addendum to Appendix 7 of the Discovery Program Plan: Program Level Requirements for the MESSENGER Extended Mission," dated 3 April 2012. Section 4.1.1 of that document summarizes full mission success for XM1 as changing the spacecraft orbital period to ~8 h, operating the spacecraft for one Earth year, and accomplishing 12 specific tasks. The orbital period was successfully adjusted to 8 h on 20 April 2012, and the spacecraft has now operated for almost half of the required Earth year. Results to date from XM1 are summarized in Table III. These baseline success criteria were included as an addendum to the original PLR for the MESSENGER mission. As of 13 September 2012, the extended mission threshold science requirements have been accomplished, and six of the twelve baseline success criteria have been accomplished:

With respect to criterion 1, as of 15 August 2012 MESSENGER has achieved 71.3 % coverage at 227 m / pixel average with 3911 three-color cubes.

With respect to criterion 2, 95 targets have been imaged at 45 m/pixel average spatial resolution.

With respect to criterion 3, by 28 August 2012, 15 hollows targets have been acquired out of 23 attempts and 6 pyroclastic targets have been acquired on 7 attempts.

With respect to criterion 4, 33 targets have been acquired in 320 images with an average resolution of 24 m/pixel.

With respect to criterion 5, as of 17 August 2012 88.0 % coverage has been achieved at 183 m/pixel average resolution (13,538 images).

With respect to criterion 6, also as of 17 August 2012, 75.0 % coverage has been achieved at 179 m / pixel average (10,654 images).

With respect to criterion 7, topographic profiles across 118 craters occupying 9 of the 10 identified regions have been obtained.

Criterion	Task	Progress
1	Image 70% of the planet in three colors at 600 m/pixel average spatial resolution	Accomplished
2	Acquire 100 sets of targeted images of hollows or pyroclastic vents at 60 m/pixel average spatial resolution.	95%
3	Acquire 20 targeted Visible and Infrared Spectrograph (VIRS) observations of hollows and pyroclastic vents at low solar incidence angle (i).	Accomplished
4	Acquire 30 sets of targeted images of young volcanic materials at 60 m/pixel average spatial resolution.	Accomplished
5	Image 70% of the planet at 250 m/pixel average spatial resolution, targeting i ~ 40–65°.	Accomplished
6	Image 70% of the planet at 250 m/pixel average spatial resolution, targeting i ~ 75–85°.	Accomplished
7	Provide topographic profiles over 10 broadly elevated regions and the floors of 50 complex impact craters, including volcanically flooded craters.	90% (elevated) 100% (floors)
8	Survey dayside and nightside exosphere emissions at an average rate of once every third orbit.	On track
9	During dawn–dusk seasons, conduct repeated observations of exospheric emissions over both poles to the maximum extent permitted by spacecraft pointing constraints.	50%
10	Conduct full-orbit, exosphere observation campaigns at equally spaced Mercury true anomalies over each of four Mercury years.	41%
11	Measure the global distribution of planetary ions and the direction of plasma flow, within operational constraints.	50%
12	Provide locations, energy spectra and pitch angles, and temporal profiles of energetic electrons across all magnetic longitudes in the northern hemisphere.	On track

Table III: MESSENGER First Extended Mission Full Success Criteria

With respect to criterion 8, ~162 dayside survey sets and ~203 nightside survey sets have been acquired, compared with 153 sets required to meet an average rate of once every third orbit. In addition, 3989 serendipitous observations on both dayside and nightside complement these dedicated observations and average about 8 per orbit.

With respect to criterion 9, observations are currently at ~50% of total expected seasonal campaigns, and at 100% success through the current date.

With respect to criterion 10, observations are currently at a 100% success rate through the current date, with 14 of 34 anticipated campaigns complete (41%).

With respect to criterion 11, the FIPS instrument is repeatedly sampling the same region, which improves the ability to distinguish temporal from spatial features, as well as to capture different space weather events. Data collection maneuver types completed to date include: 192 of 309 (62%) for magnetopause observations, 101 of 201 (50%) for central plasma sheet observations, and 34 of 50 (68%) for planned roll maneuvers.

With respect to criterion 12, a total of 372 electron events have been identified in the northern hemisphere and sorted by magnetic longitude. For each orbit routine survey plots are providing (1) electron energy flux, (2) pitch-angle distribution, (3) magnetic field magnitude, and (4) magnetic field direction for these events.

Data collection is continuing on all of these tasks in order to maximize the scientific productivity of the extended mission.

VI. SPACECRAFT STATUS

VI.I Propellant Usage and Reserves

Maneuver execution during both the primary mission and XM1 to date has been excellent, with no major anomalies and with very efficient use of propellant. The bipropellant rocket motor was used for the final time during the April 2012 maneuvers that changed MESSENGER's orbital period from 12 to 8 h, and one of the two main fuel tanks was intentionally depleted at the same time. The present estimate of remaining accessible propellant is 12.5 kg and corresponds to ~46 m/s of remaining propulsive capability, sufficient to maintain orbit through March 2015 [3].

VI.II Power

Trending of the power-generation capability of the solar arrays has yielded a well-characterized and predictable performance level of the system

remaining under the total required to operate the spacecraft and payload.

VI.III. Payload

With the exception of the Gamma-Ray Spectrometer (GRS), the MESSENGER science payload continues to function nominally and to collect data according to the prescribed observation plan. Following just over 9,502 hours of operation, the GRS cryogenic cooler has failed, rendering its primary Ge gamma-ray detector unusable for further composition observations. However, the GRS anti-coincidence shield (ACS) remains fully functional and able to detect both neutrons and energetic charged particles.

The ACS, which was designed to help filter out unwanted events from GRS data, contains more borated plastic scintillator material than the Neutron Spectrometer (NS) itself, making it the largest neutron detector on the spacecraft. It is sensitive to neutrons of all energies, offers a measurement geometry that is complementary to that of NS, and augments counting statistics.

Additionally, the ACS can be used for high-time-resolution measurements of energetic electron events. Measuring the time profile of these events with cadences shorter than previously accomplished (< 1 s) will help characterize the effect of precipitating ions and electrons on the planet's surface.

Meanwhile, measurement of the elemental composition of Mercury surface materials continues with MESSENGER's XRS.

The Mercury Laser Altimeter (MLA) remains fully functional but experienced some decrease in laser output power toward the end of the primary mission. Since then, the laser power has stabilized after operational adjustments were made to minimize the instrument's use at elevated temperatures. Laser pulse energy was measured at 20 mJ/pulse at the beginning of the mission and is now ~16 mJ/pulse. MLA has fired its laser >14 million times in 760 orbits and continues to perform nominally, with somewhat reduced range the only consequence of the lower output power.

VI.IV. Payload Response to Solar Activity

MESSENGER has so far proven to be extremely resilient to solar storms, surviving periods of increased solar activity without any lasting ill effects. The direct impact of a coronal mass ejection (CME) in June 2011 caused single-event upsets in a number of payload elements, corrupted images collected by MDIS, and triggered the autonomous safing of the XRS, GRS, and NS, but all instruments were quickly returned to normal operation. A CME in March 2012 caused radiation damage to the XRS solar monitor, but high-temperature annealing of the detector returned the unit to nominal performance. The payload continues to experience occasional upsets as solar activity continues to rise, but procedures are in place to confirm the health of the instruments and return them to nominal operations with minimal interruption in service.

VII. SUMMARY

Following six and a half years of interplanetary cruise, calibration, scientific observations during three flybys of Mercury, orbit insertion around Mercury in March 2011, and completion of its primary mission a year later, MESSENGER has, as of this writing, executed half of an extended mission of new science goals and accomplishments.

Given the current mission status, a second MESSENGER extended mission is technically achievable and promises yet another substantial advance in knowledge beyond what has been gained to date. Orbital observations during MESSENGER's XM1 are already taking particular advantage of the more active Sun, the greater fraction of time spent at low altitudes, and the ability to target a greater range of payload instruments than during the primary mission. Moreover, these additional observations are being acquired at a cost that is only a small fraction of that for a new mission.

VIII. ACKNOWLEDGMENTS

The MESSENGER Team includes hundreds of scientists, engineers, designers, technicians, support personnel, subcontractors, and managers who helped MESSENGER reach all milestones to date. We acknowledge them as well the assistance of NASA personnel and others who gave of their time to oversee and review the program to assure mission success. Details on the mission, flybys, and Mercury orbit insertion are maintained and updated at the MESSENGER website: http://messenger.jhuapl.edu/. The MESSENGER mission is supported by the NASA Discovery Program under contracts NAS5-97271 to The Johns Hopkins University Applied Physics Laboratory and contract NASW-00002 to the Carnegie Institution of Washington.

IX. REFERENCES

[1] S.C. Solomon, R.L. McNutt, Jr., R.E. Gold, D.L. Domingue, MESSENGER mission overview, Space Science Reviews, 131 (2007) 3-39.

[2] P.D. Bedini, S.C. Solomon, E.J. Finnegan, A. Calloway, B., S.L. Ensor, R.L. McNutt, Jr., B.J. Anderson, L.M. Prockter, MESSENGER at Mercury: A mid-term report, in: 62nd International Astronautical Congress, Cape Town, South Africa (2011) 9 pp.

[3] J.V. McAdams, S.C. Solomon, P.D. Bedini, E.J. Finnegan, R.L. McNutt, Jr., A.B. Calloway, D.P. Moessner, M.W. Wilson, D.T.

Gallagher, C.J. Ercol, S.H. Flanigan, MESSENGER at Mercury: From orbit insertion to first extended mission, in: 63rd International Astronautical Congress, Naples, Italy, paper IAC-12-C1.5.6 (2012) 11 pp.

[4] T.H. Choo, B.J. Anderson, P.D. Bedini, E.J. Finnegan, J.P. Skura, R.J. Steele, The MESSENGER science planning and commanding system, in: AIAA Space 2009 Conference and Exposition, American Institute of Aeronautics and Astronautics, paper AIAA-2009-6464 (2009) 11 pp.

[5] T.H. Choo, R.J. Steele, L. Nguyen, H. Nair, M. Lucks, P.D. Bedini, MESSENGER SciBox, An automated closed-loop science planning and commanding system, in: AIAA Space 2011 Conference and Exposition, American Institute of Aeronautics and Astronautics, paper AIAA-2011-7183 (2011) 6 pp.

[6] S.E. Hawkins, III, J.D. Boldt, E.H. Darlington, R. Espiritu, R.E. Gold, B. Gotwols, M.P. Grey, C.D. Hash, J.R. Hayes, S.E. Jaskulek, C.J. Kardian, M.R. Keller, E.R. Malaret, S.L. Murchie, P.K. Murphy, K. Peacock, L.M. Prockter, R.A. Reiter, M.S. Robinson, E.D. Schaefer, R.G. Shelton, R.E. Sterner, H.W. Taylor, T.R. Watters, B.D. Williams, The Mercury Dual Imaging System on the MESSENGER spacecraft, Space Science Reviews, 131 (2007) 247-338.

[7] J.O. Goldsten, E.A. Rhodes, W.V. Boynton, W.C. Feldman, D.J. Lawrence, J.I. Trombka, D.M. Smith, L.G. Evans, J. White, N.W. Madden, P.C. Berg, G.A. Murphy, R.S. Gurnee, K. Strohbehn, B.D. Williams, E.D. Schaefer, C.A. Monaco, C.P. Cork, J.D. Eckels, W.O. Miller, M.T. Burks, L.B. Hagler, S.J. DeTeresa, M.C. Witte, The MESSENGER Gamma-Ray and Neutron Spectrometer, Space Science Reviews, 131 (2007) 339-391.

[8] C.E. Schlemm, II, R.D. Starr, G.C. Ho, K.E. Bechtold, S.A. Hamilton, J.D. Boldt, W.V. Boynton, W. Bradley, M.E. Fraeman, R.E. Gold, J.O. Goldsten, J.R. Hayes, S.E. Jaskulek, E. Rossano, R.A. Rumpf, E.D. Schaefer, K. Strohbehn, R.G. Shelton, R.E. Thompson, J.I. Trombka, B.D. Williams, The X-Ray Spectrometer on the MESSENGER spacecraft, Space Science Reviews, 131 (2007) 393-415.

[9] B.J. Anderson, M.H. Acuña, D.A. Lohr, J. Scheifele, A. Raval, H. Korth, J.A. Slavin, The Magnetometer instrument on MESSENGER, Space Science Reviews, 131 (2007) 417-450.

[10] J.F. Cavanaugh, J.C. Smith, X. Sun, A.E. Bartels, L. Ramos-Izquierdo, D.J. Krebs, J.F. McGarry, R. Trunzo, A.M. Novo-Gradac, J.L. Britt, J. Karsh, R.B. Katz, A.T. Lukemire, R. Szymkiewicz, D.L. Berry, J.P. Swinski, G.A. Neumann, M.T. Zuber, D.E. Smith, The Mercury Laser Altimeter instrument for the MESSENGER mission, Space Science Reviews, 131 (2007) 451-479.

[11] W.E. McClintock, M.R. Lankton, The Mercury Atmospheric and Surface Composition Spectrometer for the MESSENGER mission, Space Science Reviews, 131 (2007) 481-521.

[12] G.B. Andrews, T.H. Zurbuchen, B.H. Mauk, H. Malcom, L.A. Fisk, G. Gloeckler, G.C. Ho, J.S. Kelley, P.L. Koehn, T.W. Lefevere, S.S. Livi, R.A. Lundgren, J.M. Raines, The Energetic Particle and Plasma Spectrometer instrument on the MESSENGER spacecraft, Space Science Reviews, 131 (2007) 523-556.

[13] S.C. Solomon, L.M. Prockter, D.T. Blewett, MESSENGER at Mercury: An introduction to the special issue of Earth and Planetary Science Letters, Earth and Planetary Science Letters, 285 (2009) 225-226.

[14] D.T. Blewett, S.A. Hauck Ii, H. Korth, Introduction to the special issue of Icarus on "Mercury after Two MESSENGER Flybys," Icarus, 209 (2010) 1-2.

[15] S.C. Solomon, R.L. McNutt, Jr, L.M. Prockter, Mercury after the MESSENGER flybys: An introduction to the special issue of Planetary and Space Science, Planetary and Space Science, 59 (2011) 1827-1828.

[16] L.R. Nittler, R.D. Starr, S.Z. Weider, T.J. McCoy, W.V. Boynton, D.S. Ebel, C.M. Ernst, L.G. Evans, J.O. Goldsten, D.K. Hamara, D.J. Lawrence, R.L. McNutt, C.E. Schlemm, S.C. Solomon, A.L. Sprague, The major-element composition of Mercury's surface from MESSENGER X-ray spectrometry, Science, 333 (2011) 1847-1850.

[17] P.N. Peplowski, L.G. Evans, S.A. Hauck, T.J. McCoy, W.V. Boynton, J.J. Gillis-Davis, D.S. Ebel, J.O. Goldsten, D.K. Hamara, D.J. Lawrence, R.L. McNutt, L.R. Nittler, S.C. Solomon, E.A. Rhodes, A.L. Sprague, R.D. Starr, K.R. Stockstill-Cahill, Radioactive elements on Mercury's surface from MESSENGER: Implications for the planet's formation and evolution, Science, 333 (2011) 1850-1852.

[18] J.W. Head, C.R. Chapman, R.G. Strom, C.I. Fassett, B.W. Denevi, D.T. Blewett, C.M. Ernst, T.R. Watters, S.C. Solomon, S.L. Murchie, L.M. Prockter, N.L. Chabot, J.J. Gillis-Davis, J.L. Whitten, T.A. Goudge, D.M.H. Baker, D.M. Hurwitz, L.R. Ostrach, Z. Xiao, W.J. Merline, L. Kerber, J.L. Dickson, J. Oberst, P.K. Byrne, C. Klimczak, L.R. Nittler, Flood volcanism in the northern high latitudes of Mercury revealed by MESSENGER, Science, 333 (2011) 1853-1856.

[19] D.T. Blewett, N.L. Chabot, B.W. Denevi, C.M. Ernst, J.W. Head, N.R. Izenberg, S.L. Murchie, S.C. Solomon, L.R. Nittler, T.J. McCoy, Z. Xiao, D.M.H. Baker, C.I. Fassett, S.E. Braden, J. Oberst, F. Scholten, F. Preusker, D.M. Hurwitz, Hollows on Mercury: MESSENGER evidence for geologically recent volatile-related activity, Science, 333 (2011) 1856-1859.

[20] B.J. Anderson, C.L. Johnson, H. Korth, M.E. Purucker, R.M. Winslow, J.A. Slavin, S.C. Solomon, R.L. McNutt, Jr., J.M. Raines, T.H. Zurbuchen, The global magnetic field of Mercury from MESSENGER orbital observations, Science, 333 (2011) 1859-1862.

[21] T.H. Zurbuchen, J.M. Raines, J.A. Slavin, D.J. Gershman, J.A. Gilbert, G. Gloeckler, B.J. Anderson, D.N. Baker, H. Korth, S.M. Krimigis, M. Sarantos, D. Schriver, R.L. McNutt, Jr., S.C. Solomon, MESSENGER observations of the spatial distribution of planetary ions near Mercury, Science, 333 (2011) 1862-1865.

[22] G.C. Ho, S.M. Krimigis, R.E. Gold, D.N. Baker, J.A. Slavin, B.J. Anderson, H. Korth, R.D. Starr, D.J. Lawrence, R.L. McNutt, Jr., S.C. Solomon, MESSENGER observations of transient bursts of energetic electrons in Mercury's magnetosphere, Science, 333 (2011) 1865-1868.

[23] S.L. Ensor, M. R. Reid, A.A. Mick, F.S. Turner, Jr., H.W. Taylor, E. Malaret, R.C. Espiritu, C.D.. Hash, Lessons learned for NASA missions delivering data to the Planetary Data System, in: AIAA Space 2012 Conference and Exposition, American Institute of Aeronautics and Astronautics, paper AIAA-2012-5257 (2012) 11 pp.

[24] N.R. Izenberg, G.M. Holsclaw, D.L. Domingue, W.E. McClintock, R.L. Klima, D.T. Blewett, M.C. Kochte, J. Helbert, M.D. D'Amore, A.L. Srprague, F. Vilas, S.C. Solomon, Ultraviolet through near-infrared reflectance variation on Mercury an the search for mineralogical telltales, Lunar and Planetary Science, 43, abstract 2365 (2012).

[25] M.T. Zuber, D.E. Smith, R.J. Phillips, S.C. Solomon, G.A. Neumann, S.A. Hauck, S.J. Peale, O.S. Barnouin, J.W. Head, C.L. Johnson, F.G. Lemoine, E. Mazarico, X. Sun, M.H. Torrence, A.M. Freed, C. Klimczak, J.-L. Margot, J. Oberst, M.E. Perry, R.L. McNutt, J.A. Balcerski, N. Michel, M.J. Talpe, D. Yang, Topography of the northern hemisphere of Mercury from MESSENGER laser altimetry, Science, 336 (2012) 217-220.

[26] D.E. Smith, M.T. Zuber, X. Sun, G.A. Neumann, J.F. Cavanaugh, J.F. McGarry, T.W. Zagwodzki, Two-way laser link over interplanetary distance, Science, 311 (2006) 53.

[27] D.E. Smith, M.T. Zuber, R.J. Phillips, S.C. Solomon, S.A. Hauck, F.G. Lemoine, E. Mazarico, G.A. Neumann, S.J. Peale, J.-L. Margot, C.L. Johnson, M.H. Torrence, M.E. Perry, D.D. Rowlands, S. Goossens, J.W. Head, A.H. Taylor, Gravity field and internal structure of Mercury from MESSENGER, Science, 336 (2012) 214-217.

[28] J.L. Margot, S.J. Peale, R.F. Jurgens, M.A. Slade, I.V. Holin, Large longitude libration of Mercury revelas a molten core, Science, 316 (2007) 710-714.

[29] M. Yseboodt, J.-L. Margot, Evolution of Mercury's obliquity, Icarus, 181 (2006) 327-337.
[30] S.J. Peale, Does Mercury have a molten core?, Nature, 262 (1976) 765-766.
[31] N.L. Chabot, C.M. Ernst, J.K. Harmon, S.L. Murchie, S.C. Solomon, D.T. Blewett, B.W. Denevi, Craters hosting radar-bright deposits in Mercury's north polar region, Lunar and Planetary Science, 43, abstract 1476 (2012).
[32] N.L. Chabot, C.M. Ernst, B.W. Denevi, J.K. Harmon, S.L. Murchie, D.T. Blewett, S.C. Solomon, E.D. Zhong, Areas of permanent shadow in Mercury's south polar region ascertained by MESSENGER orbital imaging, Geophys. Res. Lett., 39 (2012) L09204., doi:10.1029/2012GL051526.
[33] G.A. Neumann, J.F. Cavanaugh, X.L. Sun, E.M. Mazarico, D.E. Smith, M.T. Zuber, S.C. Solomon, D.A. Paige, ,Dark material at the surface of polar crater deposits on Mercury, Lunar and Planetary Science, 43, abstract 2651 (2012).
[34] D.A. Paige, M.A. Siegler, J.K. Harmon, D.E. Smith, M.T. Zuber, G.A. Neumann, S.C. Solomon, Thermal stability of frozen volatiles in the north polar region of Mercury, European Planetary Science Congress, 7, abstract EPSC2012-595 (2012).
[35] W.J. Merline, C.R. Chapman, S.C. Solomon, N.L. Chabot, R.E. Gold, S.E. Hawkins, M.S. Robinson, A program to search for vulcanoids from MESSENGER, Bulletin of the American Astronomical Society, 40, 491 (2008).
[36] D.J. Lawrence, W.C. Feldman, J.O. Goldsten, T.J. McCoy, D.T. Blewett, W.V. Boynton, L.G. Evans, L.R. Nittler, E.A. Rhodes, S.C. Solomon, Identification and measurement of neutron-absorbing elements on Mercury's surface, Icarus, 209 (2010) 195-209.
[37] J.W. Head, C.R. Chapman, D.L. Domingue, S.E. Hawkins, III, W.E. McClintock, S.L. Murchie, L.M. Prockter, M.S. Robinson, R.G. Strom, T.R. Watters, The geology of Mercury: The view prior to the MESSENGER mission, Space Science Reviews, 131 (2007) 41-84.
[38] J.W. Head, S.L. Murchie, L.M. Prockter, M.S. Robinson, S.C. Solomon, R.G. Strom, C.R. Chapman, T.R. Watters, W.E. McClintock, D.T. Blewett, J.J. Gillis-Davis, Volcanism on Mercury: Evidence from the first MESSENGER flyby, Science, 321 (2008) 69-72.
[39] J.W. Head, S.L. Murchie, L.M. Prockter, S.C. Solomon, C.R. Chapman, R.G. Strom, T.R. Watters, D.T. Blewett, J.J. Gillis-Davis, C.I. Fassett, J.L. Dickson, G.A. Morgan, L. Kerber, Volcanism on Mercury: Evidence from the first MESSENGER flyby for extrusive and explosive activity and the volcanic origin of plains, Earth and Planetary Science Letters, 285 (2009) 227-242.
[40] L.M. Prockter, C.M. Ernst, B.W. Denevi, C.R. Chapman, J.W. Head, C.I. Fassett, W.J. Merline, S.C. Solomon, T.R. Watters, R.G. Strom, G. Cremonese, S. Marchi, M. Massironi, Evidence for young volcanism on Mercury from the third MESSENGER flyby, Science, 329 (2010) 668-671.
[41] W.E. McClintock, E.T. Bradley, R.J. Vervack, R.M. Killen, A.L. Sprague, N.R. Izenberg, S.C. Solomon, Mercury's exosphere: Observations during MESSENGER's first Mercury flyby, Science, 321 (2008) 92-94.
[42] W.E. McClintock, R.J. Vervack, Jr., E.T. Bradley, R.M. Killen, N. Mouawad, A.L. Sprague, M.M. Burger, S.C. Solomon, N.R. Izenberg, MESSENGER observations of Mercury's exosphere: Detection of magnesium and distribution of constituents, Science, 324 (2009) 610-613.
[43] R.J. Vervack, Jr., W.E. McClintock, R.M. Killen, A.L. Sprague, B.J. Anderson, M.H. Burger, E.T. Bradley, N. Mouawad, S.C. Solomon, N.R. Izenberg, Mercury's complex exosphere: Results from MESSENGER's third flyby, Science, 329 (2010) 672-675.
[44] J.A. Slavin, M.H. Acuna, B.J. Anderson, D.N. Baker, M. Benna, G. Gloeckler, R.E. Gold, G.C. Ho, R.M. Killen, H. Korth, S.M. Krimigis, R.L. McNutt, L.R. Nittler, J.M. Raines, D. Schriver, S.C. Solomon, R.D. Starr, P. Trávníček, T.H. Zurbuchen, Mercury's magnetosphere after MESSENGER's first flyby, Science, 321 (2008) 85-89.
[45] J.A. Slavin, M.H. Acuna, B.J. Anderson, D.N. Baker, M. Benna, S.A. Boardsen, G. Gloeckler, R.E. Gold, G.C. Ho, H. Korth, S.M. Krimigis, R.L. McNutt, J.M. Raines, M. Sarantos, D. Schriver, S.C. Solomon, P. Trávníček, T.H. Zurbuchen, MESSENGER observations of magnetic reconnection in Mercury's magnetosphere, Science, 324 (2009) 606-610.
[46] J.A. Slavin, B.J. Anderson, D.N. Baker, M. Benna, S.A. Boardsen, G. Gloeckler, R.E. Gold, G.C. Ho, H. Korth, S.M. Krimigis, R.L. McNutt, L.R. Nittler, J.M. Raines, M. Sarantos, D. Schriver, S.C. Solomon, R.D. Starr, P.M. Trávníček, T.H. Zurbuchen, MESSENGER observations of extreme loading and unloading of Mercury's magnetic tail, Science, 329 (2010) 665-668.
[47] J.A. Slavin, B.J. Anderson, D.N. Baker, M. Benna, S.A. Boardsen, R.E. Gold, G.C. Ho, S.M. Imber, H. Korth, S.M. Krimigis, R.L. McNutt, Jr., J.M. Raines, M. Sarantos, D. Schriver, S.C. Solomon, P. Trávníček, T.H. Zurbuchen, MESSENGER and Mariner 10 flyby observations of magnetotail structure and dynamics at Mercury, J. Geophys. Res., 117 (2012) A01215, doi:10.1029/2011JA016900.
[48] J.A. Simpson, J.H. Eraker, J.E. Lamport, P.H. Walpole, Electrons and protons accelerated in Mercury's magnetic field, Science, 185 (1974) 160-166.
[49] T.P. Armstrong, S.M. Krimigis, L.J. Lanzerotti, A reinterpretation of the reported energetic particle fluxes in the vicinity of Mercury, Journal of Geophysical Research, 80 (1975) 4015-4017.
[50] G.C. Ho, R.D. Starr, R.E. Gold, S.M. Krimigis, J.A. Slavin, D.N. Baker, B.J. Anderson, R.L. McNutt, Jr, L.R. Nittler, S.C. Solomon, Observations of suprathermal electrons in Mercury's magnetosphere during the three MESSENGER flybys, Planetary and Space Science, 59 (2011) 2016-2025.
[51] G.C. Ho, S.M. Krimigis, R.E. Gold, D.N. Baker, B.J. Anderson, H. Korth, J.A. Slavin, R.L. McNutt, Jr., R.M. Winslow, S.C. Solomon, Spatial distribution and spectral characteristics of energetic electrons in Mercury's magnetosphere, J. Geophys. Res., 117 (2012) A00M04, doi:10.1029/2012JA017983.